IEEE Access
Multidisciplinary | Rapid Review | Open Access Journal

Received June 20, 2019, accepted July 8, 2019, date of publication July 10, 2019, date of current version July 30, 2019.

Digital Object Identifier 10.1109/ACCESS.2019.2928014

Experimental Demonstration of 3D Visible Light Positioning Using Received Signal Strength With Low-Complexity Trilateration Assisted by Deep Learning Technique

PENGFEI DU[1], SHENG ZHANG[1], CHEN CHEN[2], (Member, IEEE), HELIN YANG[1], (Student Member, IEEE), WEN-DE ZHONG[1], (Senior Member, IEEE), RAN ZHANG[1], AROKIASWAMI ALPHONES[1], (Senior Member, IEEE), AND YANBING YANG[3]

[1]School of Electrical and Electronic Engineering, Nanyang Technological University, Singapore 639798
[2]School of Microelectronics and Communication Engineering, Chongqing University, Chongqing 400044, China
[3]College of Computer Science, Sichuan University, Chengdu 610065, China

Corresponding author: Chen Chen (c.chen@cqu.edu.cn)

This work was supported in part by the Delta Electronics, Inc., and in part by the National Research Foundation (NRF) Singapore through the Corp Lab@University Scheme.

ABSTRACT In this paper, a 3D indoor visible light positioning (VLP) system with fast computation time using received signal strength (RSS) is proposed and experimentally demonstrated. Assisted by the deep learning techniques, the complexity of the trilateration problem is greatly reduced, and the trilateration problem can be formulated as a linear mapping leading to faster position estimation than the conventional estimation. Moreover, a new method of off-line preparation is adopted to minimize the workload of the VLP system deployment for more practical usage. The proposition is implemented on an atto-cellular VLP unit, through which the real-time performance and positioning accuracy are demonstrated and validated in a 3D positioning experiment performed in a space of $1.2 \times 1.2 \times 2$ m^3. The experimental results show that a positioning accuracy of 11.93 cm in confidence of 90% is achieved with 50 times faster the computation time compared to the conventional scheme.

INDEX TERMS Visible light communication (VLC), visible light positioning (VLP), received signal strength (RSS), light-emitting diodes (LED), deep learning.

I. INTRODUCTION

Within recent years, indoor visible light positioning (VLP) services based on visible light communication (VLC) systems become more and more attractive to researchers as the LED lighting infrastructure is being deployed worldwide [1], [2]. Indoor VLP services are able to offer higher accuracy readily than other techniques such as Wi-Fi and UWB, because the inherent characteristic of line-of-sight transmission avoids severe multipath effect which is hazardous to the achievable accuracy of positioning using Wi-Fi and UWB. Moreover, visible light is harmless to human bodies compared to radio frequencies (RFs) and ultraviolet light. It also has the benefits of cost-sharing with existing lighting infrastructure in contrast with infrared light and ultrasonic waves [3]. Consequently, many researchers are motivated to push VLP technology forward to practical use by proposing all kinds of practical VLP systems [4]–[18]. The representative works among them are summarized in table 1 in convenience of review.

As shown in table 1, almost all those works use received-signal-strength (RSS) or imaging sensor-based methods, and most of the proposed VLP systems can use one single detector to achieve high accuracy and low complexity without extra motion sensors [4], [5], [8], [11]–[16]. Despite that the imaging sensor-based methods can easily realize a VLP system of high accuracy and low complexity, such schemes are unable to integrate with high-speed VLC due to the low frame-rate of imaging sensor [4], [5], [22]. According to table 1, there are also a number of VLP systems reported recently that use

The associate editor coordinating the review of this manuscript and approving it for publication was Siddhartha Bhattacharyya.

TABLE 1. The state-of-the-art works of indoor VLP.

Literature	Method	Experiment/ Simulation	2D/3D	Accuracy	Offline workload	Other challenges and defects
[11]	RSS ratio	Experiment	2D	2.15 cm	Minor	Requiring extra photo-detectors
[12]	RSS / BP-NN	Experiment	2D	3.6 cm	Tedious	Too many reference points
[8]	RSS	Experiment	2D	1.68 cm	Tedious	Too small coverage area
[13]	RSS / TLFN	Experiment	2D	5 cm	Tedious	Too many reference points
[15]	RSS / EnKS	Experiment	2D	11.18 cm	Tedious	Not verified in 3D space
[19]	RSS / kNN-RF	Simulation	3D	19.3 cm	Tedious	Too many reference points
[16]	RSS / Bat	Simulation	3D	2.12 cm	Medium	Not verified by experiments
[20]	RSS / DE	Simulation	3D	0.69 cm	Medium	Not verified by experiments
[21]	RSS ratio	Experiment	3D	6 cm	Minor	Requiring extra photo-detectors
[5]	Imaging sensor	Experiment	3D	17 cm	Minor	Unable to integrate with high speed VLC
[6]	RSS + Accelerator	Experiment	3D	15 cm	Medium	Requiring extra sensors

RSS to achieve high accuracy and low complexity, but few of them have been experimentally verified in a 3D space [3]. Besides, as for the RSS-based VLP systems, the calibration during offline preparation is necessary [8], [10]. However, almost all of those works neglect the offline workload for users. Worse still, those VLP systems using machine-learning that though achieve good accuracy with low complexity have the least user friendliness because they require tedious offline measurements on many reference positions for the database registration or the neural-network training during deployment [12], [13], [19].

In addition, the computation speed is another critical benchmark of the indoor positioning systems as zero-latency is highly valued in some cases where high-speed intelligent vehicles are used. This target is usually reached by improving the efficiency of trilateration calculation for three-dimensional (3D) VLP using RSS. Many researchers contribute novel solutions [20], [21], [23]–[27]. However, some of the works have not been validated by experiments [20], [24], [25] or the simplifications of the calculations are still subject to complexity [21], [23]. There also exist some classic non-iterative methods, some of which even achieve an excellent computation efficiency by providing closed-form formulations for the trilateration problem [26], [27]. However, they are not applicable in the case of VLP because they need to know distance between receivers and transmitters through various range measurements before solving the trilateration. In contrast, VLP using RSS usually gives the RSS measurements with unknown distances and unknown heights based on the channel modeling [14]. Hence, it is unable to measure the distance directly. Meanwhile, some researchers adopt machine-learning techniques to realize fingerprinting based 3D VLP system using RSS so as to completely circumvent the trilateration calculation. Unfortunately, such a system has tedious offline workload and terrible user friendliness as stated above [19], [28]. Worse still, the users have to run the tedious offline measurements every time when the LED transmitter, the receiver or the environment is changed, which is not appropriate for practical usage.

In order to address the challenges above, this paper proposes and experimentally demonstrates a practical 3D VLP system, which retains the distance estimation using RSS and combines machine learning to simplify the trilateration solution so that the computation speed can be substantially increased with minimum offline preparation work. The offline preparation can be conducted involving at most two reference positions regardless of quantities of LED lamps. The main contributions of our work are listed as below:

- We for the first time propose and experimentally verify a new and practical 3D RSS-based VLP system using only two reference positions for offline preparation.
- We for the first time apply deep learning techniques in VLP systems using RSS for faster computing speed.
- We investigate the optimal layer size of artificial neural network (ANN) for the deep learning-based position estimator to balance the performance and cost.

The rest of our paper is organized as follows. In Section II, the proposed VLP system is presented in details, ranging from systematic overview to the deep learning parameters. Section III demonstrates the experimental work validating the feasibility of the proposed VLP system in comparison with the conventional 3D VLP system using RSS. Finally, the summary of the paper is given in Section IV.

II. PRINCIPLE

This section introduces the principle of the proposed VLP system, including the overall system model, RSS-based distance estimation and simplified trilateration solution assisted by deep learning techniques.

A. SYSTEM MODEL

The RSS-based VLP system is depicted in Fig. 1. As shown in Fig. 1(a), the VLP system is in the form of cellular at the transmitter side to realize a full coverage inside a room in which a certain number of neighboring LED lamps are grouped into one cellular unit. As is commonly known, the coverage of one VLP cellular unit is much smaller than the one using radio frequency, and hence the concept of cellular VLP system is actually redefined as atto-cellular VLP system [2]. As the proposition adopts the frequency division multiple access (FDMA) scheme, the signal generator

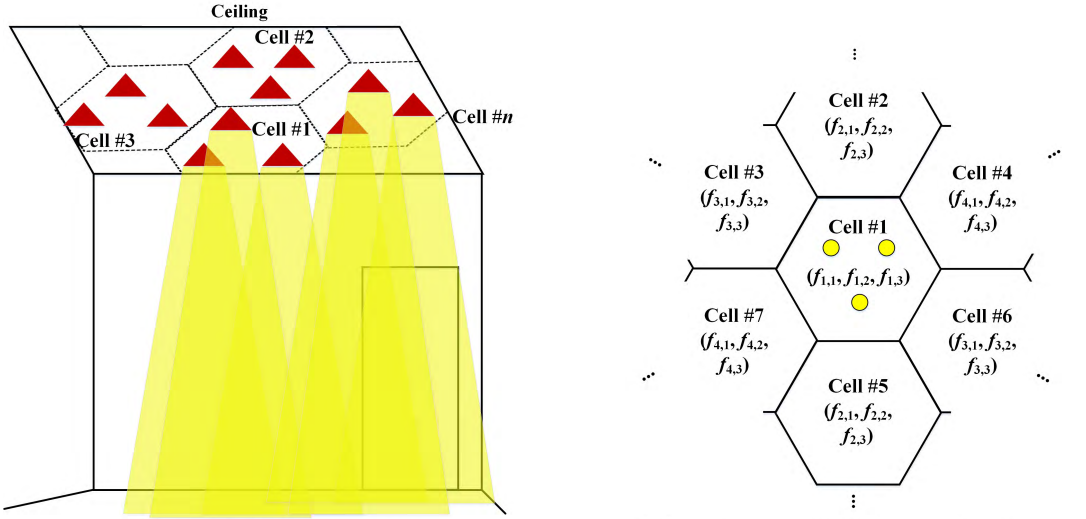

(a) Atto-cellular VLP transmitting system

(b) Frequency reuse in the hexogonal cell pattern

FIGURE 1. Schematic of the (a) atto-cellular VLP transmitting system and (b) the frequency reuse in the hexagonal cell pattern.

generates sinusoidal waves with unique frequencies as modulation signals for every LED transmitter in each atto-cells. In order to mitigate the interference between neighboring atto-cells while retaining high spectrum efficiency, the frequency reuse and hexagonal cell pattern design are both introduced [29]. As shown in Fig. 1(b), each atto-cell has three LED lamps carrying three different carriers, and different groups of carrier frequencies are allocated to the neighboring cells. Without loss of generality, Cell #1 is assumed to be placed in the center of the targeted coverage surrounded by other six cells. Among those six cells, the ones that are angular symmetric with respect to Cell #1, share the same frequency use. Under the same rule, the cells can be duplicated for a bigger coverage area. In this way, only four groups of carriers need to be reserved for the whole positioning network. The details of one cell unit are revealed by Fig. 2(a). As shown in Fig. 2(a), the bias tees are deployed to generate DC biased sinewave signals to drive LEDs. The DC component is used for illumination, while the sinewave signal component amplified by the current booster is used to make LED flicker for signal transmission. It is noteworthy that the flickering is not sensitive to human eyes due to the high frequency. In this way, the lighting function of LEDs are not affected and consequently the LEDs can be simultaneously used for illumination and positioning. Fig. 2(b) illustrates the VLP receiver for users consisting of an avalanche photodetector coupled with optical blue filter and a digital localization module. The photodetector simultaneously collects the signal from all LED transmitters and the blue filter forces the photodetector to collect blue light solely as the other spectrum is limited in bandwidth by phosphor coating. The digital localization module is composed of a digitizer, an RSS estimator and a position estimator. The digitizer firstly converts the analogue output of photodetector into digital signals. The RSS estimator subsequently measures the signal strength at predetermined frequencies, i.e., the signal strength from individual LED transmitters according to the FDMA scheme. The measurement is conducted by means of fast Fourier transformation (FFT) on the digitized signal. Finally, the position is given by the position estimator based on the signal attenuation model and the trilateration method, whereas the deep learning technique is adopted for performance enhancement.

B. DISTANCE ESTIMATION BASED ON RSS

In addition to introducing the channel attenuation model similar as the state-of-art work, this section also formulates the distance estimation based on RSS for practical usage utilizing the measured Lambertian order and the measured RSS at the reference positions.

To start with, the channel modeling is formulated including the derivation of LED irradiation model. The pattern irradiated by a real LED lamp composing multiple LED chips is considered herein. The received signal of the k-th receiver at the position p_k from the j-th LED chip in Tx-i is characterized as

$$RSS_{j,i,p_k} = \frac{(m_i+1)}{2\pi d_{j,i,p_k}^2} A_r \cos^{m_i}(\beta_{j,i,p_k}) F_s(\alpha_{j,i,p_k}) \times L_g(\alpha_{j,i,p_k}) \cos(\alpha_{j,i,p_k}) TSS_{j,i}. \quad (1)$$

where $TSS_{j,i}$ is the transmitted positioning signal strength from the j-th LED chip in Tx-i and RSS_{j,i,p_k} is the received strength of the positioning signal from $TSS_{j,i}$ at the position p_k; m_i is the order number of Lambertian radiation pattern

of the LED chip of Tx-i, which will be measured during the offline preparation for the VLP system; d_{j,i,p_k} is the distance between the j-th LED chip in Tx-i and the receiver at the position p_k; A_r is the sensitive area of photodetector; β_{j,i,p_k} is the incidence angle of visible light from the j-th LED chip in Tx-i, and α_{j,i,p_k} is the emission angle of the j-th LED chip in Tx-i relative to the receiver at the position p_k; F_s is the gain of the optical blue filter and $Lg(\alpha_{j,i,p_k})$ is the gain of the optical concentrator.

Regarding the real LED lamp that usually consists of a number of LEDs, the received signal from Tx-i is written as

$$RSS_{i,p_k} = \sum_{j=1}^{N} \left[\frac{m_i+1}{2\pi d_{j,i,p_k}^2} A_r \cos^{m_i}(\beta_{j,i,p_k}) F_s(\alpha_{j,i,p_k}) \times L_g(\alpha_{j,i,p_k}) \cos(\alpha_{j,i,p_k}) TSS_{j,i} \right], \quad (2)$$

where N is the number of LED chips in Tx-i. As the receiver herein is targeted to use plastic filter without lens, the gain of the blue filter and the optical concentrator are independent from the incidence angle. Hence, Eq. (2) is equivalent to

$$RSS_{i,p_k} = A_r \cdot F_s \cdot L_g \times \sum_{j=1}^{N} \frac{m_i+1}{2\pi d_{j,i,p_k}^2} \cos^{m_i}(\beta_{j,i,p_k}) \cos(\alpha_{j,i,p_k}) TSS_{j,i}. \quad (3)$$

As the LED chips in one lamp are close to each other, d_{j,i,p_k} can be approximated to be equal to d_{i,p_k} which denotes the distance between Tx-i and the receiver at position p_k. Without loss of generality, the transmitted positioning signal strength of each LED chip is assumed to be equal. Let TSS denote the transmitted positioning signal strength shared by all LED chips, we have

$$RSS_{i,p_k} \triangleq A_r \cdot F_s \cdot L_g \cdot \frac{m_i+1}{2\pi d_{i,p_k}^2} \cdot TSS \times \sum_{j=1}^{N} \cos^{m_i}(\beta_{j,i,p_k}) \cos(\alpha_{j,i,p_k}). \quad (4)$$

The receiver is assumed to be fixed and face the ceiling vertically. This assumption is valid for many typical scenarios including VLP for autonomous ground vehicles (AGVs) in a smart workshop and VLP for robots in a smart home. Due to this assumption, we have,

$$\cos(\beta_{j,i,p_k}) = \cos(\alpha_{j,i,p_k}) = \frac{h_{p_k}}{d_{i,p_k}}, \quad (5)$$

where h_{p_k} is the vertical distance from ceiling to the receiver at position p_k. Consequently, Eq. (4) is rewritten as

$$RSS_{i,p_k} \approx A_r \cdot F_s \cdot L_g \cdot \frac{m_i+1}{2\pi d_{i,p_k}^2} \cdot TSS \cdot N \cdot \left(\frac{h_{p_k}}{d_{i,p_k}}\right)^{m_i+1}. \quad (6)$$

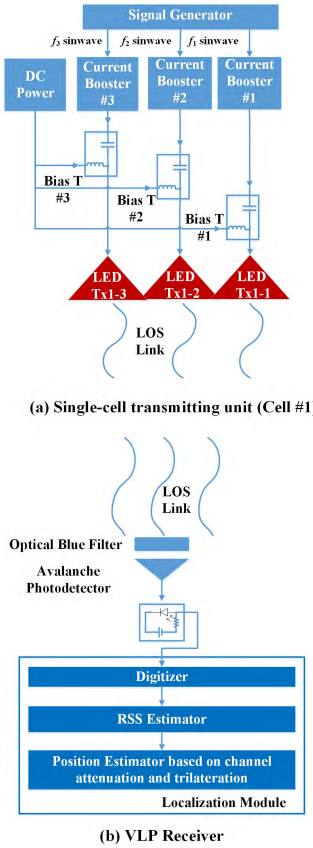

FIGURE 2. Schematic of the (a) single-cell transmitting unit and (b) the VLP receiver.

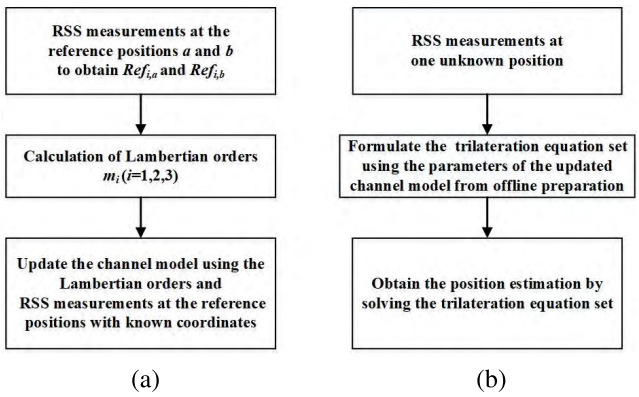

FIGURE 3. Workflow of (a) offline preparation and (b) online position estimation of the proposed VLP system.

Using C to denote the constant terms $(A_r \cdot F_s \cdot L_g \cdot TSS \cdot N/2\pi)$, Eq. (6) can be simplified as

$$RSS_{i,p_k} \approx C \cdot (m_i+1) \cdot \frac{h_{p_k}^{m_i+1}}{d_{i,p_k}^{m_i+3}}. \quad (7)$$

According to Eq. (7), d_{i,p_k}, h_{p_k} and consequently the position can be estimated once the constant C and m_i of the specific VLP system is determined. However, Zheng *et al.* [10] and Alam *et al.* [30] have pointed out that m_i in practice

is not close to the theoretical value and that each LED lamp has slightly different values for m_i. Hence, it is necessary to perform the offline preparation to measure m_i using the reference positions with known position information. Differing from the previous work [10], [30], [31], our proposed offline preparation needs as minimum as two reference positions without any information on the number or the transmitted power strength of lamps. The only requirement is that the span of the two reference positions should necessarily represent the localization coverage or the range of SNR. The workflow of the offline preparation is depicted in Fig. 3(a). As we can see in Fig. 3(a), there are three steps to fulfill the offline preparation.

Firstly, the RSS values from Tx-i at the reference positions a and b are measured. Denoted by $Ref_{a,i}$ and $Ref_{b,i}$, respectively, the RSS values can be formulated as,

$$\begin{cases} Ref_{i,a} = RSS_{i,p_a} = C \cdot (m_i + 1) \cdot \dfrac{h_{p_a}^{m_i+1}}{d_{i,p_a}^{m_i+3}} \\ Ref_{i,b} = RSS_{i,p_b} = C \cdot (m_i + 1) \cdot \dfrac{h_{p_b}^{m_i+1}}{d_{i,p_b}^{m_i+3}}. \end{cases} \tag{8}$$

where d_{i,p_a} and d_{i,p_b} denote the known distance between the LED Tx-i and the receiver placed at the reference positions a and b, respectively. Assuming $h_{p_a} = h_{p_b}$ for convenience of explanation but without loss of generality, Eq. (8) can be manipulated as

$$\frac{Ref_{i,a}}{Ref_{i,b}} = \left(\frac{d_{i,p_b}}{d_{i,p_a}}\right)^{m_i+3}. \tag{9}$$

Subsequently, the Lambertian order m_i of LED Tx-i is calculated by

$$m_i = \log_{\frac{d_{i,p_b}}{d_{i,p_a}}}\left(\frac{Ref_{i,a}}{Ref_{i,b}}\right) - 3. \tag{10}$$

Last but not the least, the data m_i, d_{i,p_a}, d_{i,p_b}, h_{i,p_a}, h_{i,p_b}, $Ref_{i,a}$ and $Ref_{i,b}$ are stored in a database for positioning operation. In this way, the channel model can be adequately close to the practical scenario using the data included above, hence the online position estimation can be more precise facilitated by the updated channel model.

The online positioning operation exploiting the data obtained during offline preparation is illustrated by Fig. 3(b). As we can see in Fig. 3(b), the RSS value from Tx-i at the unknown position p_k is measured at first, which is given by Eq. (7). Combining Eq. (7) and (8), it can be further expressed as,

$$RSS_{i,p_k} = Ref_{i,a} \cdot \left(\frac{h_{p_k}}{h_{p_a}}\right)^{m_i+1} \cdot \left(\frac{d_{p_a,i}}{d_{p_k,i}}\right)^{m_i+3}. \tag{11}$$

Regarding the position estimation by a single-cell unit with three LED lamps, Eq. (11) can be expanded to three equations. Substituting the unknown coordinates into Eq. (11), the trilateration equation sets can be given by

$$\begin{cases} RSS_{1,p_k} = Ref_{1,a} \cdot \left(\dfrac{r_3 - T_{1,n}}{h_{p_a}}\right)^{\left(\log_{\frac{d_{1,p_b}}{d_{1,p_a}}}\left(\frac{Ref_{1,a}}{Ref_{1,b}}\right)\right)-2} \\ \qquad \times \left(\dfrac{d_{p_a,1}}{\sqrt{\sum_{n=1}^{3}(r_n - T_{1,n})^2}}\right)^{\log_{\frac{d_{1,p_b}}{d_{1,p_a}}}\left(\frac{Ref_{1,a}}{Ref_{1,b}}\right)} \\ RSS_{2,p_k} = Ref_{2,a} \cdot \left(\dfrac{r_3 - T_{2,n}}{h_{p_a}}\right)^{\left(\log_{\frac{d_{2,p_b}}{d_{2,p_a}}}\left(\frac{Ref_{2,a}}{Ref_{2,b}}\right)\right)-2} \\ \qquad \times \left(\dfrac{d_{p_a,2}}{\sqrt{\sum_{n=1}^{3}(r_n - T_{2,n})^2}}\right)^{\log_{\frac{d_{2,p_b}}{d_{2,p_a}}}\left(\frac{Ref_{2,a}}{Ref_{2,b}}\right)} \\ RSS_{3,p_k} = Ref_{3,a} \cdot \left(\dfrac{r_3 - T_{3,n}}{h_{p_a}}\right)^{\left(\log_{\frac{d_{3,p_b}}{d_{3,p_a}}}\left(\frac{Ref_{3,a}}{Ref_{3,b}}\right)\right)-2} \\ \qquad \times \left(\dfrac{d_{p_a,3}}{\sqrt{\sum_{n=1}^{3}(r_n - T_{3,n})^2}}\right)^{\log_{\frac{d_{3,p_b}}{d_{3,p_a}}}\left(\frac{Ref_{3,a}}{Ref_{3,b}}\right)} \end{cases}, \tag{12}$$

where (r_1, r_2, r_3) is the position coordinate to be estimated, n represents the n-th dimension and $(T_{j,1}, T_{j,2}, T_{j,3})$ is the j-th LED's coordinate. Conventionally, the position estimator adopts iteration-based methods such as Newton-Raphson method and Levenberg-Marquard method to solve the equation numerically hence to complete the position estimation. However, the solution takes much longer time than expected if the initial values are inappropriately chosen. To address the concern, we propose a new deep-learning based estimator simplifying the trilateration solution which will be elaborated in the following subsection.

C. SIMPLIFIED TRILATERATION SOLUTION ASSISTED BY DEEP-LEARNING-BASED POSITION ESTIMATOR

As stated above, the ANN based deep learning technique is applied in the proposed system to build a novel position estimator which fulfills the position estimation instead of directly solving the trilateration equation sets with numerical methods [32]. In this section, building the deep learning-based position estimator to simplify the trilateration solution is elaborated.

The structure of the proposed ANN is illustrated in Fig. 5. Similar to the conventional position estimator, the input of ANN is the set of RSS values from all LED lamps, and the output is the corresponding position coordinates. As shown in Fig. 5, there are three inputs of RSS and three outputs corresponding to the coordinate (r_1, r_2, r_3). There are n hidden layers, and the activation function is denoted by f. The offline preparation is twofold. The first stage is to use the two reference positions to obtain Lambertian orders as in Eq. 10. After the calibrated irradiation pattern and channel model are fully acquired, the second stage is initiated by training the ANN

with the theoretical RSS values derived from the calibrated channel modeling to acquire those parameters of ANN, such as $W_{i,j}$, $b_{i,j}$, etc. As the first stage of offline preparation has fully calibrated the irradiation pattern and channel model, a large dataset containing true positions and corresponding RSS values can be derived numerically based on Eq. (12) to train the ANN. The dataset for training herein contains 80631 RSS samples along with the respective position coordinates. The locations of the samples form a grid with 5-cm resolution in the space of $2.5\times2.5\times1.5$ m^3. We resort the class of MLPRegressor from Scikit-learn library in Python [33] to train ANN with the dataset collected numerically as stated above. Overall, we train the ANN using backpropagation algorithm with 70% of the dataset, and we validate and test the ANN with 10% and 20% of the dataset, respectively. The learning rate is set as a constant value of 0.001. All the crucial parameters of ANN and the deep-learning setup are listed in Table 2. The architect and the scale of ANN and alpha parameter for L2 regularization are optimally determined.

TABLE 2. Parameters of ANN and deep learning setup.

Training algorithm	Activation function
Backpropagation	Relu
Solver	**Percentage of samples for training**
Adam	70%
Total number of neurons	**Number of hidden layers**
700	5
Hidden layer size	**Alpha parameter**
(140,140,140,140,140)	1e-5
Regularization	**Percentage of samples for validation**
L2	10%
Learning rate	**Percentage of samples for testing**
Constant as 0.001	20%

Among those parameters, we mainly focus on the total neuron numbers and the number of hidden layers. As deep learning technique involves multiple hidden layers and a great number of neurons, it is important to define a suitable architect and an appropriate scale of ANN because too many neurons or hidden layers may lead to overfitting while insufficient neurons may fail to achieve good results due to the lack of degrees of freedom [34]. We test quite a few ANNs with multiple hidden layers to obtain the optimal hidden layer size of the ANN. Feeding the dataset for test (i.e., 20% of the 80631 samples) into the ANNs to be evaluated, we calculate and compare the mean error and max error of the output as metrics for ANN performance evaluation. In addition, ANN with single hidden layer is also investigated to quantify the advantage of deep learning technique. According to Fig. 4(a), it can be found that ANN with multiple hidden layers (i.e., the deep learning technique) outperforms that with a single hidden layer. With the same total neuron number applied, ANN with 4 hidden layers can roughly achieve half of the mean error as compared to ANN with a single

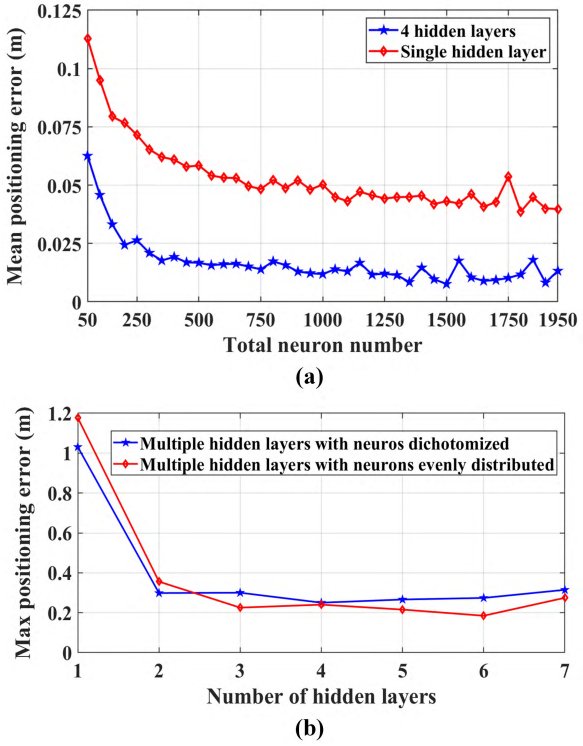

FIGURE 4. Training performance vs. (a) total neuron numbers and (b) number of hidden layers.

hidden layer. It implies that the deep learning techniques can fit the non-linearity in the trilateration problem more precisely. The result of Fig. 4(a) has also explained the motivation of utilizing deep learning methods in our works: to decrease the computation time while retaining the best positioning accuracy. It is true that other learning methods can also achieve this goal under certain configurations. However, using deep learning method can readily achieve better positioning accuracy. In preliminary study of our scenario, it is also found that the total number of neurons for ANNs with multiple hidden layers generally affects the overall performance regardless of the number of hidden layers. Therefore, we firstly opt to study the ANN with 4 hidden layers to obtain the optimal total neuron numbers. As observed in Fig. 4(a), the average positioning error is significantly reduced with increase of total neuron numbers when less than 700. The performance is almost the same when the total neuron number exceeding 700, thus we opt to use 700 neuron numbers to build the optimal ANN. Subsequently, we investigate and compare the specific hidden layer size to acquire the optimal architect of ANN for our scenario. Fig. 4(b) depicts the training performance of the ANNs with the optimal total neuron number but different numbers of hidden layers. Two typical layer architects are also considered. One is in the form of dichotomization (e.g., (350, 175, 88, 88)), while the other evenly distribute neurons into each layer (e.g., (175, 175, 175, 175)). Generally, the difference of their performances is minor. Taking both

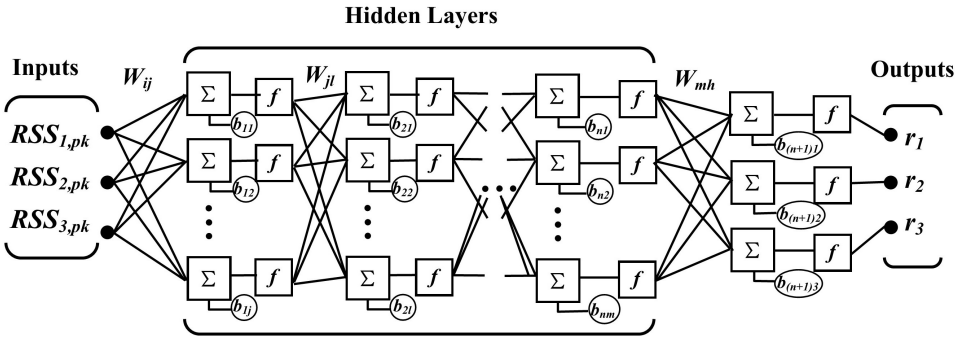

FIGURE 5. The structure of proposed ANN.

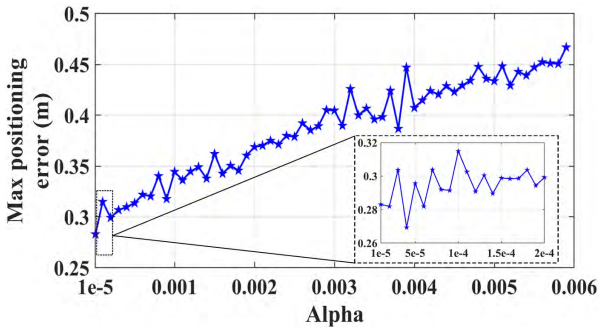

FIGURE 6. Training performance vs. alpha parameters.

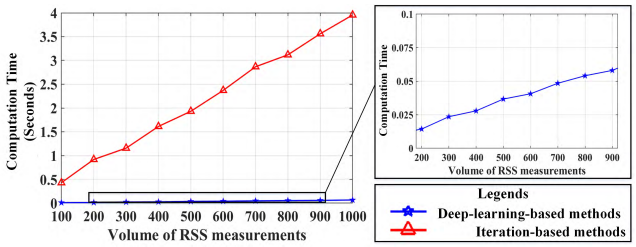

FIGURE 7. Online consumed time of trilateration solution vs. the number of RSS measurement sets comparing deep-learning-based method and the conventional iteration-based method.

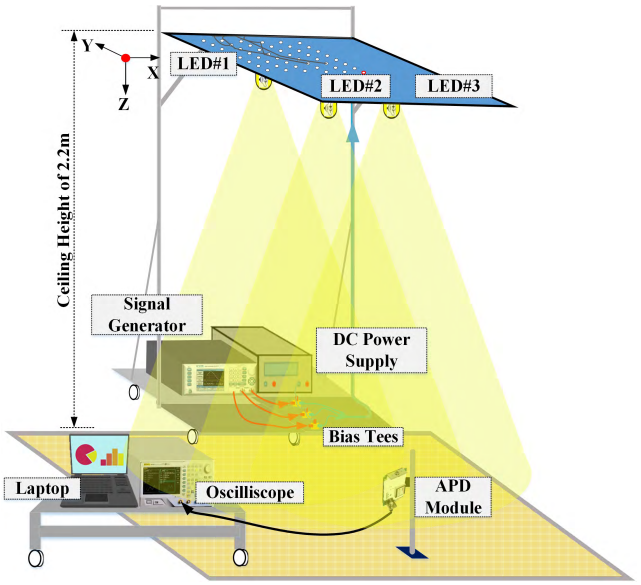

FIGURE 8. Experimental setup.

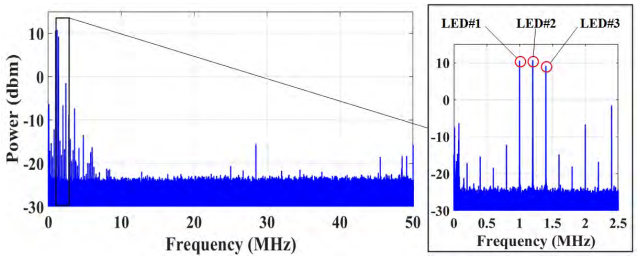

FIGURE 9. Electrical spectrum of the signal received at the coordinate of (0.4560, 0.1966, 2.006).

effectiveness and complexity into account, we eventually opt for layer size (140, 140, 140, 140, 140) to build the ANN.

In order to mitigate the overfitting effect, we also investigate the optimal alpha parameter for L2 regularization term which penalizes weights with large magnitudes [33]. Likewise, we use the max positioning error from test dataset as the metrics for performance evaluation. The positioning errors with different alpha parameters are concluded in Fig. 6. It is evident that the max error increases with alpha value, thus we opt for 1e-5 for alpha to build the ANN with optimal architect.

During the design, the real-time performance is analyzed by comparing with the typical numerical method, i.e., Newton-Raphson method, in terms of computation time. It should be noted that this comparison is just to show the superior of our proposed method over the iterative methods in terms of computation time. Hence, we just opt for Newton Raphson as a typical and representative iterative method for comparison. As is commonly known, the time complexity for Newton-Raphson method is $O(m \times n^3)$, while for deep learning-based solution, the worst case of the ANN-based mapping is only $O(N_{neurons}^2)$ [35], [36]. Herein, m is the iteration times, n is the number of equations, and $N_{neurons}$ is the number of neurons of the trained ANN. Given that the total number of neurons is constant for an ANN, $O(N_{neurons}^2) = O(1)$, thus the complexity is far less than the Newton-Raphson

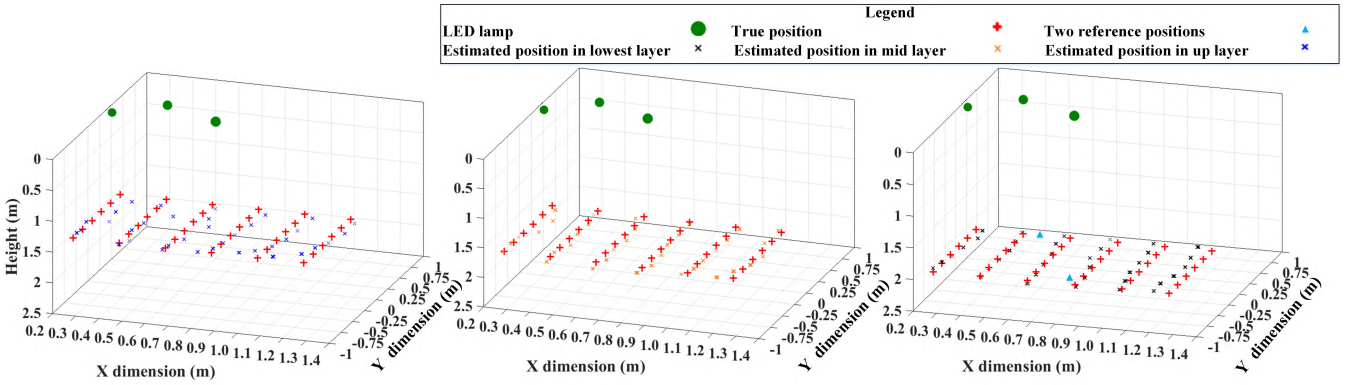

FIGURE 10. 3D Position estimation at heights of (a) 1.094 m, (b) 0.794 m and (c) 0.494 m.

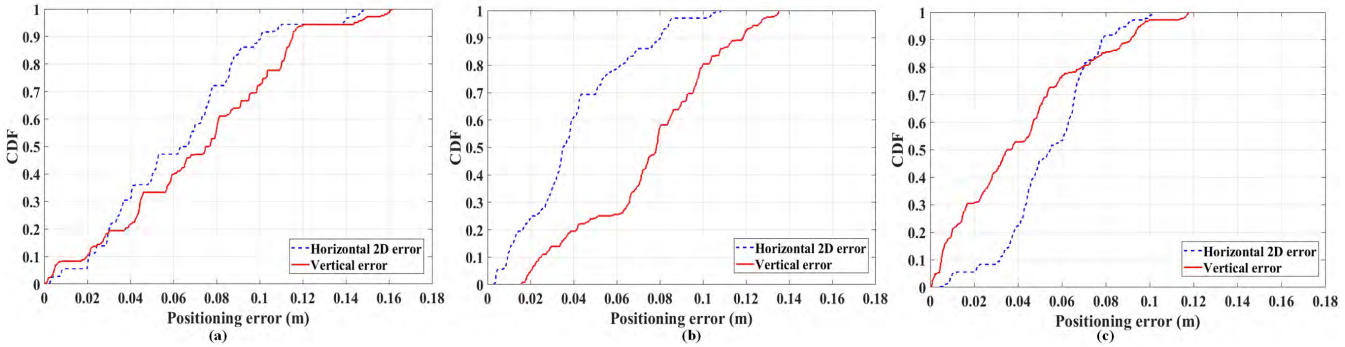

FIGURE 11. Horizontal 2D positioning error and vertical error at heights of (a) 1.094 m, (b) 0.794 m and (c) 0.494 m.

method [36], [37]. Moreover, the deep-learning-assisted solution is theoretically advantageous than the Newton-Raphson method, because it is non-iterative and its time complexity is not related with problem size. To further quantify the advantage, we directly simulate and compare the time consumed by the trilateration solution using Newton-Raphson method and the simplified trilateration solution using deep learning technique. Fig. 7 shows that the computation time of conventional trilateration solution using Newton-Raphson method can be extremely shortened by one order of magnitude thanks to the deep learning technique. In conclusion, the deep learning-based position estimator can fully achieve the function of conventional estimator with much faster speed. In addition, we should note that the computation time for comparison herein is only the online consumed time. It is acknowledged that the deep-learning technique is superior over the conventional computation methods regarding the online computation time but inevitably costs more time during offline preparation. Fortunately, the extra offline training hardly adds extra labor intensity, and the training is not necessarily frequent because the parameters of the deep neural network are stable once the deployment completed. Therefore, our proposition is worth the effort especially for the scenarios where zero-latency is appreciated.

III. EXPERIMENTAL DEMONSTRATION

A. EXPERIMENTAL SETUP

The atto-cellular VLP system for experimental investigation is implemented. The signal flow is same as illustrated in Fig. 2, and Fig. 8 is the photograph of the experimental setup. Three LED (Lumiled LXK8-PW50-0016) lamps were used as transmitters which were mounted on a horizontal panel with a height of 2.2 m. The power of each LED lamp was 9 W (27 W for one cell unit), and the divergence angle was 120°. The DC bias point was 200 mA. The illumination level at the receiving plane under the cell unit was 380 lux which has reached the standard of indoor illumination. The modulation index was set as 0.5. As we constrained DC bias point and modulation index into the linear region, nonlinearity was not obviously observed. Given that the frequency response of the LED chips used in the experiment is only 7 MHz, we opted to allocate carrier frequencies of 1 MHz, 1.2 MHz and 1.4 MHz to LED#1, LED#2 and LED#3, respectively. Using those relatively low RF frequencies is beneficial to achieve reasonable SNR and hence acceptable positioning accuracy. The RF carriers are generated from a signal generator (Spectrum M4x.6622-x4) and amplified by the current boosters (Analog Devices Inc. AD811 and Burr-Brown BUF634) before they are used to

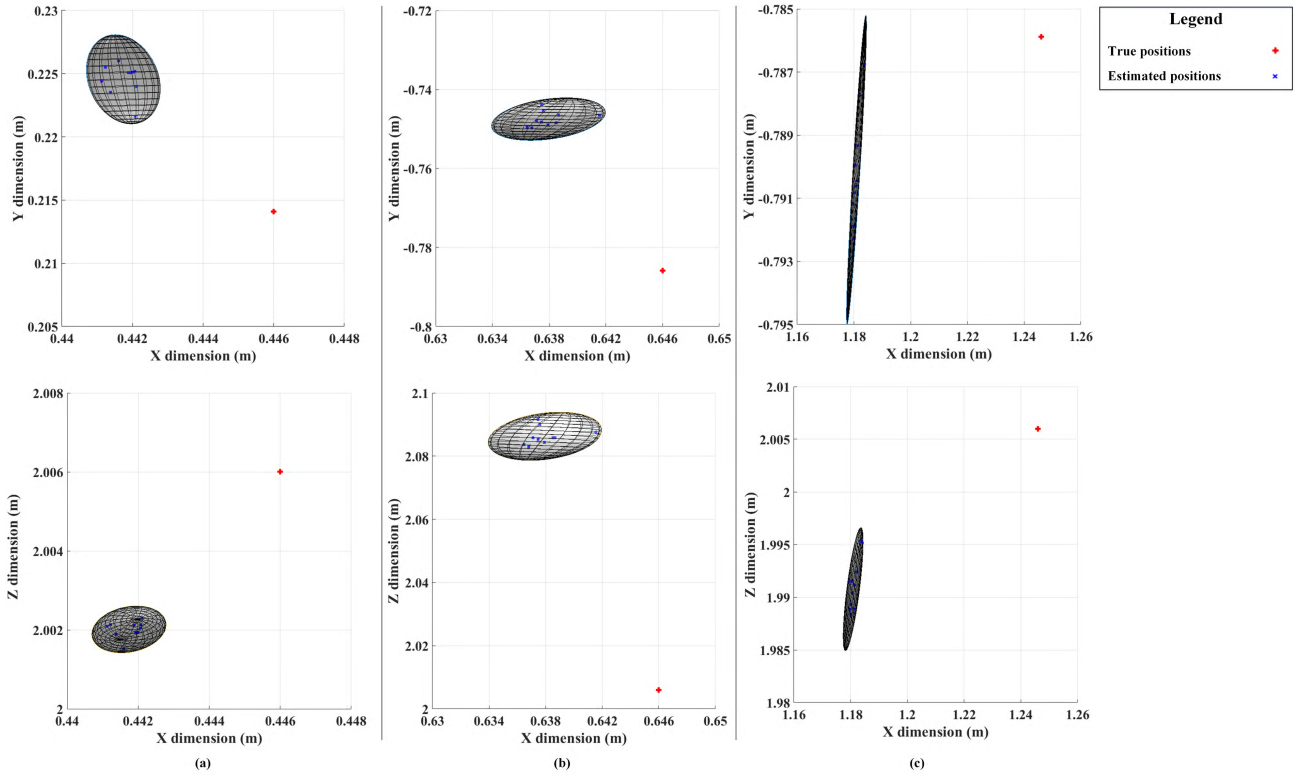

FIGURE 12. 95% confidence error ellipsoids at (a) the center point (0.446, 0.2141, 2.0060), (b) the edge point (0.646, −0.7859, 2.0060) and (c) the corner point (1.2460, −0.7859, 2.0060).

drive the LEDs. The receiver which is mounted on a trolley is composed of an avalanche photo-diode module (Hamamatsu S8664-50K), an oscilloscope (Tektronix MSO3102) and a laptop. The avalanche photo-diode module is fixed facing the ceiling without tilting angles.

B. EXPERIMENTAL RESULTS AND DISCUSSION

As shown in Fig 8, the origin of the system was on the ceiling. As is commonly known, trilateration depends strongly on the LEDs' locations. Hence, the optimal LED arrangement from the previous works was adopted for our experiments [38], [39]. The coordinates of the LEDs were (0.425, 0.375, 0), (0.675, 0.125, 0) and (0.225, 0.125, 0), respectively. Fig. 9 shows the spectrum measured at one reference position where the receiver has equidistance between the LED lamps. As seen in Fig. 9, the power received from different lamps are still different although the distances from the receiver to the lamps are equal, which is mainly due to the inclined frequency response. Worse still, the frequency responses are inevitably and slightly different among LED lamps according to observations on the received power of LED#1 and LED#2. In turn, it also explains the necessity of performing the offline preparation and maximizing the usage of ratio RSS. In the experiment, it is noteworthy that only two reference positions (marked by cyan triangles in Fig. 10) are involved in our proposition to perform the offline preparation. The coordinates of those two reference positions were (0.4460, 0.2141, 2) and (0.6660, −0.9059, 2), respectively. The effort of offline preparation has been effectively minimized. According to the offline preparation, the calibrated Lambertian order for the three lamps is 1.7131, 2.0937 and 2.1129, respectively. It can be seen that the calibrated Lambertian order can be so different even for same LED lamps. This is most likely due to two causes: 1) the imperfect parameter settings in the realistic setups compared to the theoretical propagation model; 2) and the possible bias errors of measuring RSS in the offline preparation. For instance, the gain of optical receiver is likely to slightly change with the incidence angles leading to imperfect removal of C in Eq. 9. All those errors will be reflected by the calculated Lambertian order. On the other hand, the possible bias errors of measuring RSS on single frequency will be also reflected by the calibrated Lambertian order.

As constrained by the experimental environment, we only choose around one quarter of the illumination coverage of LED lamps to conduct experiment, the area of which is around 1.2×2 m^2. Considering the ceiling height, the 3D positioning space is $1.2\times1.2\times2$ m^3, and the actual coverage for practical usage will be even larger. During the experiment, $6 \times 6 \times 3$ locations were estimated (marked by red crosses in Fig. 10) with 10 times for each position. The position estimations are shown in Fig. 10, which are grouped into three vertical layers marked by different colors. The heights of the

TABLE 3. Comparisons among state-of-the-art works of 3D indoor VLP.

Literature	Method	Coverage	Accuracy	Remarks / Disadvantages compared to our proposed work
[6]	RSS + Accelerator	1.4×2.5 m^2	15 cm	Requiring extra sensors
[7]	RSS / BP-NN	3×3 m^2	12 cm	Tedious offline preparation due to more reference points
[5]	Imaging sensor	1.0×1.5 m^2	17 cm	Unable to integrate with high speed VLC
Our proposed work	RSS / Deep-learning assisted trilateration	1.2×1.2 m^2	8.92 cm	Estimated coverage with equivalent accuracy is 2.4×2.4 m^2

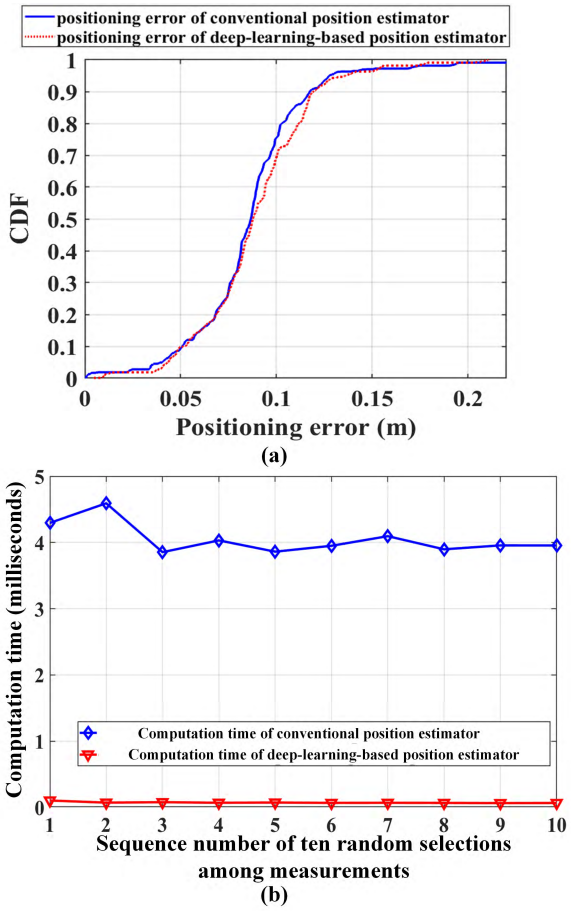

FIGURE 13. (a) Positioning error and (b) Computation time of position estimation for our proposition and the conventional 3D positioning method.

vertical layers were 0.494 m, 0.794 m and 1.094 m, respectively. As can be observed, most of the position estimations are close to the true positions. The positioning errors of those three heights are further concluded by Fig. 11 in terms of horizontal errors and vertical errors. In most cases, Z-coordinate is worse than the X-Y coordinate, but the 90% vertical error is still less than 12cm, which is still in an acceptable range. Furthermore, we investigated the error ellipsoid at few typical positions at the center, edge and corner of the coverage area. The X-Y projection and X-Z projection of 95% confidence error ellipsoids in Fig. 12 were plotted based on 10 times measurements at those positions. According to Fig. 12, a conclusion can be reached: the bias error of position estimation is a major concern, and the positioning performance in the central area is much better that in the edge or the corner of the coverage area.

The overall error of localization is also summarized in Fig. 13(a) as compared to the localization error of the conventional scheme using the traditional trilateration method [8]. It can be seen that the mean and the 90% errors are 8.92 and 11.93 cm, respectively, which are almost same as the localization accuracy of the conventional scheme. In addition, the coverage area with such an equivalent positioning accuracy can be estimated up to 2.4×2.4 m^2 because the area for testing is just one quarter section of the illumination coverage. More importantly, our proposition successfully achieves 50 times faster computing speed than the conventional system, as illustrated by Fig. 13(b). As stated in Section II, the improvement in the online consumed time is important to those scenarios where zero-latency is highly valued. In conclusion, the proposed system significantly shortens the online computation time due to the adoption of the deep learning techniques, and reduces the labor intensity due to the proposed work of minimum offline preparation, while retaining high positioning accuracy, as compared to the conventional scheme.

IV. CONCLUSION

In this paper, a practical 3D VLP system using RSS with low-complexity trilateration assisted by deep learning is proposed to address: 1) the complicated solution to the trilateration problem; 2) the shortcoming of the previous existing scheme relying on tedious offline preparation. The proposed VLP system is elaborated by separately introducing the channel modeling, the Lambertian order measurement in offline preparation and the online position estimation simplified by deep learning technique along with theoretical derivations. Moreover, the proposed simplified position estimation is theoretically proved to outperform the existing iteration-based trilateration solution in terms of the time complexity. Finally, the whole proposition is realized as an atto-cellular 3D VLP system. Compared with the conventional VLP using RSS, the feasibility of the proposed scheme has been adequately validated by a 3D positioning experiment performed in a space of $1.2\times1.2\times2$ m^3. The experimental results show that a positioning accuracy of 11.93 cm in confidence of 90% can be achieved with 50 times faster computation time as compared to the conventional system.

The proposed scheme featuring the minimum offline preparation work retains the distance estimation using RSS and incorporates deep learning techniques to simplify the trilateration solution, and hence the real-time performance can be easily guaranteed. Moreover, our work is further compared with the state-of-art of indoor 3D VLP system as

shown in table 3. Overall, our proposed work can achieve an equivalent accuracy but with low hardware complexities and minimum offline workloads. In conclusion, our proposed work is a competitive option among them. It is noteworthy that capabilities of utilizing deep learning can go beyond what this work has revealed. For instance, our works can be further modified to address the complicated calculation of arbitrary tilting angles and sparse online training for accuracy enhancement. Both exciting prospects will be discussed in our future works.

REFERENCES

[1] J. Luo, L. Fan, and H. Li, "Indoor positioning systems based on visible light communication: State of the art," *IEEE Commun. Surveys Tuts.*, vol. 19, no. 4, pp. 2871–2893, 4th Quart., 2017. doi: 10.1109/COMST.2017.2743228.

[2] M. Biagi, S. Pergoloni, and A. M. Vegni, "LAST: A framework to localize, access, schedule, and transmit in indoor VLC systems," *J. Lightw. Technol.*, vol. 33, no. 9, pp. 1872–1887, May 1, 2015. doi: 10.1109/JLT.2015.2405674.

[3] E. W. Lam and T. D. C. Little, "Visible light positioning: Moving from 2D planes to 3D spaces," *Chin. Opt. Lett.*, vol. 17, no. 3, 2019, Art. no. 030604.

[4] R. Zhang, W.-D. Zhong, K. Qian, and D. Wu, "Image sensor based visible light positioning system with improved positioning algorithm," *IEEE Access*, vol. 5, pp. 6087–6094, 2017.

[5] B. Zhu, J. Cheng, Y. Wang, J. Yan, and J. Wang, "Three-dimensional VLC positioning based on angle difference of arrival with arbitrary tilting angle of receiver," *IEEE J. Sel. Areas Commun.*, vol. 36, no. 1, pp. 8–22, Jan. 2018.

[6] M. Yasir, S.-W. Ho, and B. N. Vellambi, "Indoor positioning system using visible light and accelerometer," *J. Lightw. Technol.* vol. 32, no. 19, pp. 3306–3316, Oct. 1, 2014. doi: 10.1109/JLT.2014.2344772.

[7] S. Zhang, P. Du, C. Chen, W.-D. Zhong, and A. Alphones, "Robust 3D indoor VLP system based on ANN using hybrid RSS/PDOA," *IEEE Access*, vol. 7, pp. 47769–47780, 2019.

[8] B. Lin, X. Tang, Z. Ghassemlooy, C. Lin, and Y. Li, "Experimental demonstration of an indoor VLC positioning system based on OFDMA," *IEEE Photon. J.*, vol. 9, no. 2, Apr. 2017, Art. no. 7902209.

[9] S. Cincotta, C. He, A. Neild, and J. Armstrong, "High angular resolution visible light positioning using a quadrant photodiode angular diversity aperture receiver (QADA)," *Opt. Express*, vol. 26, no. 7, pp. 9230–9242, 2018. doi: 10.1364/OE.26.009230.

[10] H. Zheng, Z. Xu, C. Yu, and M. Gurusamy, "A 3-D high accuracy positioning system based on visible light communication with novel positioning algorithm," *Opt. Commun.*, vol. 396, pp. 160–168, Aug. 2017. doi: 10.1016/j.optcom.2017.03.058.

[11] X. Yu, J. Wang, and H. Lu, "Single LED-based indoor positioning system using multiple photodetectors," *IEEE Photon. J.*, vol. 10, no. 6, Dec. 2018, Art. no. 7909108.

[12] C.-W. Hsu, S. Liu, F. Lu, C.-W. Chow, C.-H. Yeh, and G.-K. Chang, "Accurate indoor visible light positioning system utilizing machine learning technique with height tolerance," in *Proc. Opt. Fiber Commun. Conf. Expo. (OFC)*, Mar. 2018, pp. 1–3.

[13] X. Guo, F. Hu, N. R. Elikplim, and L. Li, "Indoor localization using visible light via two-layer fusion network," *IEEE Access*, vol. 7, pp. 16421–16430, 2019.

[14] Y. Wu, Z. Guo, X. Liu, Y. Xian, and W. Guan, "High precision and high speed of three-dimensional indoor localization system based on visible light communication using improved bacterial colony chemotaxis algorithm," *Proc. SPIE*, vol. 58, no. 3, 2019, Art. no. 036103.

[15] Y. Zhuang, Q. Wang, M. Shi, P. Cao, L. Qi, and J. Yang, "Low-power centimeter-level localization for indoor mobile robots based on ensemble kalman smoother using received signal strength," *IEEE Internet Things J.*, to be published.

[16] L. Huang, P. Wang, Z. Liu, X. Nan, L. Jiao, and L. Guo, "Indoor three-dimensional high-precision positioning system with bat algorithm based on visible light communication," *Appl. Opt.*, vol. 58, no. 9, pp. 2226–2234, 2019.

[17] S. Li, S. Shen, and H. Steendam, "A positioning algorithm for VLP in the presence of orientation uncertainty," *Signal Process.*, vol. 160, pp. 13–20, Jul. 2019.

[18] B. Zhou, A. Liu, and V. Lau, "Robust visible light-based positioning under unknown user device orientation angle," in *Proc. 12th Int. Conf. Signal Process. Commun. Syst. (ICSPCS)*, Cairns, QLD, Australia, Dec. 2018, pp. 1–5.

[19] H. Tran and C. Ha, "Fingerprint-based indoor positioning system using visible light communication—A novel method for multipath reflections," *Electronics*, vol. 8, no. 1, p. 63, 2019.

[20] Y. Wu, X. Liu, W. Guan, B. Chen, X. Chen, and C. Xie, "High-speed 3D indoor localization system based on visible light communication using differential evolution algorithm," *Opt. Commun.*, vol. 424, pp. 177–189, Oct. 2018.

[21] S. H. Yang, H. S. Kim, Y. H. Son, and S. K. Han, "Three-dimensional visible light indoor localization using AOA and RSS with multiple optical receivers," *J. Lightw. Technol.*, vol. 32, no. 14, pp. 2480–2485, Jul. 15, 2014.

[22] Y. Xu, Z. Wang, P. Liu, J. Chen, S. Han, C. Yu, and J. Yu, "Accuracy analysis and improvement of visible light positioning based on VLC system using orthogonal frequency division multiple access," *Opt. Express*, vol. 25, no. 26, pp. 32618–32630, 2017.

[23] B. Chen, J. Jiang, W. Guan, S. Wen, J. Li, and Y. Chen, "Performance comparison and analysis on different optimization models for high-precision three-dimensional visible light positioning," *Proc. SPIE*, vol. 57, no. 12, 2018, Art. no. 125101.

[24] S. H. Yang, E. M. Jeong, D. R. Kim, H. S. Kim, Y. H. Son, and S. K. Han, "Indoor three-dimensional location estimation based on LED visible light communication," *Electron. Lett.*, vol. 49, no. 1, pp. 54–56, Jan. 2013.

[25] N. Li, Y. Qiao, T.-T. Zhang, and Y. Lu, "Dead-zone-free three-dimensional indoor positioning method based on visible light communication with dimensionality reduction algorithm," *Proc. SPIE*, vol. 57, no. 3, 2018, Art. no. 036114.

[26] W. Navidi, W. S. Murphy, Jr., and W. Hereman, "Statistical methods in surveying by trilateration," *Comput. Statist. Data Anal.*, vol. 27, no. 2, pp. 209–227, 1998.

[27] F. Thomas and L. Ros, "Revisiting trilateration for robot localization," *IEEE Trans. Robot.*, vol. 21, no. 1, pp. 93–101, Feb. 2005.

[28] I. Alonso-González, D. Sánchez-Rodríguez, C. Ley-Bosch, and M. A. Quintana-Suárez, "Discrete indoor three-dimensional localization system based on neural networks using visible light communication," *Sensors*, vol. 18, no. 4, p. 1040, 2018.

[29] V. H. M. Donald, "Advanced mobile phone service: The cellular concept," *Bell System Tech. J.*, vol. 58, no. 1, pp. 15–41, Jan. 1979.

[30] F. Alam, B. Parr, and S. Mander, "Visible light positioning based on calibrated propagation model," *IEEE Sensors Lett.*, vol. 3, no. 2, Feb. 2019, Art. no. 6000204.

[31] S. W. Ho, J. Duan, and C. S. Chen, "Location-based information transmission systems using visible light communications," *Trans. Emerg. Telecommun. Technol.*, vol. 28, no. 1, 2017, Art. no. e2922. doi: 10.1002/ett.2922.

[32] H. B. Demuth, M. H. Beale, and O. De Jess, *Neural Network Design*. Boston, MA, USA: Martin Hagan, 2014.

[33] L. Buitinck, G. Louppe, and M. Blondel, "API design for machine learning software: Experiences from the scikit-learn project," in *Proc. ECML PKDD Workshop, Lang. Data Mining Mach. Learn.*, 2013, pp. 108–122.

[34] R. Caruana, S. Lawrence, and C. L. Giles, "Overfitting in neural nets: Backpropagation, conjugate gradient, and early stopping," in *Proc. Adv. Neural Inf. Process. Syst.*, 2001, pp. 402–408.

[35] C. Ferreira, *Designing Neural Networks Using Gene Expression Programming*. Berlin, Germany: Springer, 2006.

[36] S. S. Haykin, *Neural Networks and Learning Machines*, vol. 3, Upper Saddle River, NJ, USA: Pearson 2009.

[37] J. J. Steil, "Backpropagation-decorrelation: Online recurrent learning with O(N) complexity," in *Proc. IEEE Int. Joint Conf. Neural Netw.*, Jul. 2004, pp. 843–848.

[38] S. Zhang, W.-De Zhong, P. Du, and C. Chen, "Experimental demonstration of indoor sub-decimeter accuracy VLP system using differential PDOA," *IEEE Photon. Technol. Lett.*, vol. 30, no. 19, pp. 1703–1706, Oct. 1, 2018.

[39] Z. Sheng, W.-D. Zhong, D. Pengfei, C. Chen, and D. Wu, "PDOA based indoor visible light positioning system without local oscillators in receiver," in *Proc. Conf. Lasers Electro-Opt. Pacific Rim (CLEO-PR)*, Jul. 2017, pp. 1–3.

PENGFEI DU received the B.Eng. degree in mechanical engineering from Sichuan University, Chengdu, China, in 2011, and the Ph.D. degree in optical engineering from Tsinghua University, Beijing, China, in 2016. He is currently a Research Fellow with the School of Electrical and Electronics Engineering, Nanyang Technological University. His current research interests include LiDAR, visible light positioning, Li-Fi, and quantum detection.

SHENG ZHANG received the B.Eng. degree from the School of Optical and Electronic Information, Huazhong University of Science and Technology, China, in 2015. He is currently pursuing the Ph.D. degree with the School of Electrical and Electronic Engineering, Nanyang Technological University, Singapore. His research interests include indoor localization and tracking systems, and visible light communication and positioning.

CHEN CHEN received the B.S. and M.Eng. degrees from the University of Electronic Science and Technology of China, Chengdu, China, in 2010 and 2013, respectively, and the Ph.D. degree from Nanyang Technological University, Singapore, in 2017.

He was a Postdoctoral Researcher with the School of Electrical and Electronic Engineering, Nanyang Technological University, from 2017 to 2019. He is currently an Assistant Professor with the School of Microelectronics and Communication Engineering, Chongqing University, China. His research interests include visible light communications, LiFi, visible light positioning, optical access networks, and digital signal processing.

Dr. Chen received the Best Paper Award at the IEEE Photonics Global Conference, in 2015. He was a recipient of the outstanding reviewer certificates from *Optical Fiber Technology* (Elsevier) and *Digital Signal Processing* (Elsevier), in 2017 and 2018, respectively. He received the Publons Peer Review Awards in both Engineering and Physics, in 2018. He was also a co-recipient of the IET Optoelectronics Premium Award, in 2018.

HELIN YANG (S'15) received the B.S. and M.S. degrees from the School of Telecommunications and Information Engineering, Chongqing University of Posts and Telecommunications, in 2013, and 2016, respectively. He is currently pursuing the Ph.D. degree with the School of Electrical and Electronic Engineering, Nanyang Technological University, Singapore. His current research interests include wireless communication, visible light communication, and resource management.

WEN-DE ZHONG (SM'03) received the Ph.D. degree from the University of Electro-Communications, Japan, in 1993.

He was a Postdoctoral Fellow with NTT Network Service and System Laboratories, Japan, from 1993 to 1995. He was a Senior Research Fellow with the Department of Electrical and Electronic Engineering, University of Melbourne, Australia, from 1995 to 2000. In 2000, he joined Nanyang Technological University, as an Associate Professor, where he became a Full Professor, in 2009. He is currently a Professor with the School of Electrical and Electronic Engineering, Nanyang Technological University, Singapore. He has coauthored more than 250 refereed journal and conference papers. His current research interests include visible light communication/positioning, optical fiber communication systems and networks, optical access networks, and signal processing.

Dr. Zhong is also an Associate Editor of the IEEE ACCESS and an Editor of *Unmanned Systems*. He has served on the organizing and/or the technical program committees for numerous international conferences, including ECOC, ICC, GLOBECOM, OECC, ICICS, and ICOCN.

RAN ZHANG received the B.Eng. degree in communication engineering from Jilin University, China, in 2014. She is currently pursuing the Ph.D. degree with the Interdisciplinary Graduate School (IGS), Nanyang Technological University, Singapore. Her research interests include sensor fusion, indoor localization and tracking systems, and visible light communication and positioning.

AROKIASWAMI ALPHONES received the B.Tech. degree from the Madras Institute of Technology, Chennai, India, in 1982, the M.Tech. degree from IIT Kharagpur, Kharagpur, India, in 1984, and the Ph.D. degree in optically controlled millimeter-wave circuits from the Kyoto Institute of Technology, Kyoto, Japan, in 1992. From 1997 to 2001, he was with the Centre for Wireless Communications, National University of Singapore, Singapore, where he was involved in research on optically controlled passive/active devices. Since 2001, he has been with the School of Electrical and Electronic Engineering, Nanyang Technological University. He is currently an Associate Professor with the School of Electrical and Electronic Engineering, Nanyang Technological University. He is also a Program Coordinator for research. He has 30 years of research experience. He has authored and presented over 250 technical papers in peer-reviewed international journals/conferences. His current research interests include electromagnetic analysis on planar RF circuits and integrated optics, microwave photonics, metamaterial-based leaky wave antennas, and wireless power transfer technologies. He was a Visiting Fellow of the JSPS, Japan, from 1996 to 1997. He was involved in many IEEE flagship conferences held in Singapore. He was the General Chair of APMC 2009 and MWP 2011. He is also the Chairman of the IEEE Singapore Section.

YANBING YANG received the B.E. and M.E. degrees from the University of Electronic Science and Technology of China, China, and the Ph.D. degree in computer science and engineering from Nanyang Technological University, Singapore. He is currently an Associate Research Professor with the College of Computer Science, Sichuan University, China. His research interests include the IoT, visible light communication, visible light sensing, as well as their applications.